ARTICLES

Journal of Semiconductors
(2021) 42, 122801
doi: 10.1088/1674-4926/42/12/122801

Novel synthesis of cerium oxide nano photocatalyst by a hydrothermal method

Fowziya Shaik Ali[1], Faisal Al Marzouqi[2], A. Afroos Banu[1], M. Ismail Fathima[3], A. R. Mohamed Jahangir[4], K. Mohamed Rafi[5], and A. Ayeshamariam[6, †]

[1]Department of Chemistry, Khadir Mohideen College, Adirampattinam 614701 (Affiliated to Bharathidasan University, Tiruchirappalli), India

[2]Department of Process Engineering, International Maritime College Oman, Falaj Al Qabail, Suhar, Oman

[3]Department of Physics, Arul Anandar College (Auto), Karumathur, Madurai 625514, India

[4]Biyaq Oilfield Services LLC, Mina Al Fahal PC, 116, Muscat, Sultanate of Oman

[5]Research Department of Botany, Jamal Mohamed College (Auto) (Affiliated to Bharathidasan University, Thiruchirappalli) – 620020, India

[6]Research Department of Physics, Khadir Mohideen College (Affiliated to Bharathidasan University, Thiruchirappalli) Adirampattinam – 614701, India

Abstract: Crystalline cubic cerium oxide nano particles have been synthesized from cerium (III) nitrate (Ce $(NO_3)_3.6H_2O$) and sodium hydroxide by a hydrothermal method. The effect of three different molar ratios of the NaOH precipitating agent on structural, optical, and photo catalytic activity was investigated. The synthesized cerium oxide nano particles were characterized by X-ray diffraction (XRD), a UV–vis spectrometer, scanning electron microscope (SEM), energy-dispersive X-ray spectroscopy (EDAX), Raman spectroscopy and X-ray photo electron spectroscopy (XPS). According to the findings, hydrothermally synthesized cerium oxide NPs have a high efficiency for photocatalytic degradation of methylene blue when exposed to UV light. Environmental water pollution is the major issue of the atmosphere. To get fresh water, humans could search the resources to purify the water in simple way and degradation is the one of the methods to purify salt water.

Key words: cerium oxide; nano particles; photo catalysis; hydrothermal process

Citation: F S Ali, F Al Marzouqi, A A Banu, M I Fathima, A R M Jahangir, K M Rafi, and A Ayeshamariam, Novel synthesis of cerium oxide nano photocatalyst by a hydrothermal method[J]. *J. Semicond.*, 2021, 42(12), 122801. http://doi.org/10.1088/1674-4926/42/12/122801

1. Introduction

One-dimensional oxide material and its nano structure have attracted great attention because of their remarkable applications in many fields of opto-electronic and electrochemical devices[1]. Great progress has been achieved on the different synthesis approaches for one dimensional nano structure and usually they require surfactant and precipitant in a series of complicated procedures. Cerium oxide (CeO_2) is one of the excellent oxides materials and most important for its promising application as catalyst[2].

Various controlled synthetic agents were already reported and indicate that various formation process of CeO_2 nano structure and it involves nucleation and aggregation of different sizes of this oxide nano structure[3]. This cerium (IV) oxide source materials possess high ionic and electronic conductivity and have attracted a lot of attention because its desired size and shape can be easily produced to control processing parameter like pH, reaction temperature, reaction time, precipitants concentration and types of solvents[4].

CeO_2 and its doped nano structure have attracted much attention due to improvement in redox properties, transport properties and the surface-to-volume ratios with respect to bulk material[5]. There is a lack of information on the effect of different precipitants to study the structure, morphology and optical properties by hydrothermal processing and how precursor concentration affects the different doped ceria and its oxide nano particles[6]. Like those composites, catalysts are usually provided to prepare active materials independently its emission and excitation wavelength[7]. Elimination of organic pollutants through reduction and oxidation reaction has been applied to provide outstanding photo chemical activity in a number of reactions, CO_2 reduction as well as in a series of degradation reaction concerning several pollutants such as formaldehyde, phenol, toluene and organic dyes[8–10]. Controlled morphology is a facile method to prepare CeO_2 sphere with high efficiency on photo catalysis under visible light. Different catalysts are widely used to control photo catalytic behaviour and that materials act as an oxygen buffer by releasing and up taking oxygen through redox process and increases efficiency of catalyst by enlarging the air to fuel operating window[11].

The active molecules were prepared by various chemical routes. In recent years, along with, the application of nanoscience using various metals such as magnesium oxide (MgO), nanosilicon (Si), silver oxide (Ag_2O), zinc oxide (ZnO), copper oxide (CuO), gold (Au), titanium dioxide (TiO_2) and calcium oxide (CaO) were studied[12]. The one of the anatase phase TiO_2 metal oxide nano particles was synthesised facile solutions phase method without use of surfactant from titani-

Correspondence to: A Ayeshamariam, ayeshamariamkmc@gmil.com
Received 16 APRIL 2021; Revised 10 JUNE 2021.

um isopropoxide and different alcoholic medium (methanol, ethanol, propanol and butanol) and also demonstrated their excellent performance in photo degrading methylene blue and bisphenol aqueous solution by using UV-A light irradiation[13].

Qi *et al.* synthesized a series of fullerene (C_{60})-modified anatase TiO_2 (a-TiO_2) nanocomposites by an effortless solution phase method and also investigated photocatalytic degradation of methylene blue (MB) under UV-A light irradiation[14]. Zhang *et al.* successfully reported the photodegradation of methylene blue (MB) solution under a simulated solar light irradiation by Er^{3+}:$YAlO_3$ loaded. The relationship between the volume of loading and the rate of deterioration was also studied[15]. Sim *et al.* compared unimodal and bimodal nano porous silica structures in Ag NPs and discovered that the bimodal nano porous structure had a higher absorption potential and faster adsorption rate[16].

Recently, ceria nanoparticles were synthesised by various methods such as combustion[17], the spray diffusion method[18], the reverse micelles/surfactant assisted method[19], flame spray pyrolysis[20], the sol-jel method[21], homogeneous precipitation[22], the sono chemical-microwave method[23] and hydrothermal method[24–27]. The hydrothermal method has fascinated and created a lot of interest to produce nanoparticles of a desired size and shape, owing to the ease controlling of processing parameter like solution pH, reaction time, reaction temperature, solute concentration and solvent used[4]. Nanoparticles with small grains and high purity can be achieved due to homogeneous nucleation in hydrothermal synthesis[28].

The successful preparation method of nanoparticles consolidates its atmosphere that small particles condense from the vapour and then filled with oxygen which promotes rapid oxidation of oxide nanoparticles. It has strong particles which has agglomeration during the oxidation step and difficulty on controlling the concentration of the precursor, although its different morphological nano structure such as nano rods, nano wire, and nano cube has already been reported and synthesized by various methods[29].

This work describes hydrothermal synthesis which is an attractive method for the preparation of crystalline cerium (IV) oxide nanoparticles. It has a simple crystal structure and it has good solid solubility and many dopants[30]. To the best of our knowledge one step-controlled synthesis of CeO_2 and its doping nano structure has not been reported to date. Hence, the paper describes a simple surfactant-free, hydrothermal synthesis route to the synthesis of CeO_2 nano structure[31, 32].

Many researchers focus on the selection of active components and the role of rare-earth oxides as catalysts. However, there is little research on the effects of pore structure, particle size, crystal surface area and other adsorption mechanisms on the performance of catalysts and the structure–activity relationship. Such improvement mechanisms could be due to the improved light absorption in the visible-light region induced by localized surface plasmon resonance (LSPR) and the efficient interfacial separation and transport of charge carriers in $Ag/Ag_2S/Bi_2MoO_6$[33]. The extraordinary photocatalytic property is ascribed to the Z-scheme hetero-structure with unique core–shell architecture that realizes compactly interfacial contact between the components for efficient separation of photo-excited carriers, strong visible-light absorption, as well as possesses the strong oxidation ability of the photo-excited hole, and the high reduction capacity of photo-excited electrons[34]. Superoxide free radicals (O_2^-) and photo-excited holes (h^+) were determined to be the main active species in degrading MB dyes by the results of absorption of photo catalysts[35]. The study on photocatalytic mechanism demonstrates that superoxide free radicals (O_2^-) and photo-generated hole (h^+) are dominantly responsible for the MB dye degradation, therefore, huge absorption potential is utilized as a durable and highly active photocatalyst for wastewater treatment[36].

2. Experimental methodology

2.1. Materials requirement

Cerium oxide NPs were synthesized using analytical-grade cerium (III) nitrate ($Ce(NO_3)_3{\cdot}6H_2O$, Sigma Aldrich, 99%) and sodium hydroxide (NaOH, Sigma Aldrich, 99%) without further purification and ultra-pure water.

The use of hydrothermal synthesis reduced the number of intermediate products. The technique of ceria synthesis has a significant impact on CeO_2's photocatalytic activity. In the photocatalytic process carried out under visible and solar light, a rise in the specific surface area, a decrease in the pore size, and an increase in the quantity of oxygen vacancies resulted in a high rate of hydrogen generation.

2.2. Synthesis

Analytical grade cerium nitrate hexa hydrate ($Ce(NO)_3{\cdot}6H_2O$) source material was dissolved in 75 mL of ultra-pure water (1 mmol solution of 0.4342 g was added), and the solution was stirred at room temperature for 15 min. 0.24, 0.20 and 0.16 g of NaOH pellets dissolved in ultra-pure water while the drop wise addition of NaOH solution with continuous stirring (stirring was about 30 min) been made. After 30 min, white precipitant was obtained and the pH noted was 12.8 ue to the dissolved oxygen present in air changes Ce(III) to Ce(IV)[37]. By using hydrothermal synthesis we got the fine powder under the autoclave with a Teflon lining, which was kept at 160 °C for 12 h. After that autoclave was cooled to room temperature, the yellow precipitate was collected by centrifugation for 6 min with 7500 rpm. And the collected powder was washed with ultra-pure water and ethanol and dried at 80 °C for 12 h. The collected powder was calcined at 350 °C for 1 h to obtain for further crystallization. Different molar concentrations of NaOH (4MMOL, 5MMOL and 6MMOL) were prepared and its mechanisms were reported here[38].

$$Ce^{3+} + 3OH^- \rightarrow Ce(OH)_3, \tag{1}$$

$$4Ce(OH)_3 + 2H_2O + O_2 \rightarrow 4Ce(OH)_4, \tag{2}$$

$$Ce(OH)_4 \rightarrow CeO_2 + 2H_2O. \tag{3}$$

2.3. Characterization

The crystalline properties of the synthesized nanoparticles were studied by XRD using a Bench X MiniFlex600 equipped with graphite monochromatized Cu Kα radiation

(λ = 1.540 Å).

An accelerating voltage of 40 kV and emission current of 30 mA were adopted for the measurements. In addition to XRD, Raman spectroscopy measurements were also performed to confirm the structure of the nanoparticles. The dispersive Raman spectrometer (Bruker SENTERA 200LX model) employs a solid-state laser with an excitation wavelength of 532 nm. Typical Raman measurements were carried out in the spectral range between wave number 200 and 1100 cm^{-1}. The morphology of the crystal was characterized by a field emission scanning electron microscope (FESEM). The FESEM measurements were performed by a JSM-7800F (JOEL, JAPAN). The maximum working voltage of 15 kV and 10 mm working distance was used during the measurement. The FESEM equipment was also furnished with an EDX spectrometer that was used for elemental analysis. X-ray photoelectron spectroscopy (XPS) measurements carried on a multi-probe X-ray photoelectron spectroscopy (XPS) (Omicron Nanotechnology, Germany). XPS measurements were analysed as individual components using Casa XPS software (Casa Software Ltd). The binding energies of the obtained data were calibrated with respect to carbon C 1s peak at 284.6 eV. Absorption spectra of the samples in the diffused reflectance spectrum (UV–vis DRS) mode were recorded in the wavelength range of 200-1000 nm using a spectrophotometer (Lambda 650S-perk Elmer). From the adsorption edge, the band gap values were calculated by extrapolation.

2.4. Photocatalytic activity

Photocatalytic activity of pure CeO_2 nano particle were examined by the rate of degradation of MB under the effect of UV-B irradiation. All photocatalytic reactions were performed out in a photocatalytic reactor system, which consists of a cylindrical borosilicate glass reactor vessel with volume of 250 mL, a cooling water jacket, and a UV-B lamp (8 watts medium pressure mercury lamp, Institute of Electric Light Source, Beijing) positioned axially at the centre as a visible light. The reaction temperature was kept at 25 °C by circulating the cooling water. A special glass frit as an air diffuser was fitted at the reactor to uniformly spread the air into the solution. The reaction suspension was prepared freshly for each cycle by mixing 250 mg of catalyst with 250 mL of methylene blue at a starting concentration of 5 mg/L. After the degradation reaction, filtration was done for all samples using a syringe and syringe filter 0.45 μm to remove any precipitated particles. The filtrate was analysed by an UV–vis spectrometer (UC-2450-SHIMADZU). The MB's maximum characteristic absorption wavelength was positioned[39].

3. Results and discussion

3.1. X-ray diffraction analysis

The synthesized CeO_2 NPs was characterized by using X-ray diffractometer to study the structural properties of the sample. The XRD patterns of as synthesized sample was shown in Fig. 1. By using JCPDS file no: 81-0792, it was in good agreement with results and its diffractions are equal to (111), (200), (220), (400) and (311) planes. The diffraction peak absorbed in Fig. 1 can be indexed to pure cubic CeO_2 and its lattice parameter is a = 5.5425 Å. By using Debye Scherrer's formula, the average grain size was calculated[40].

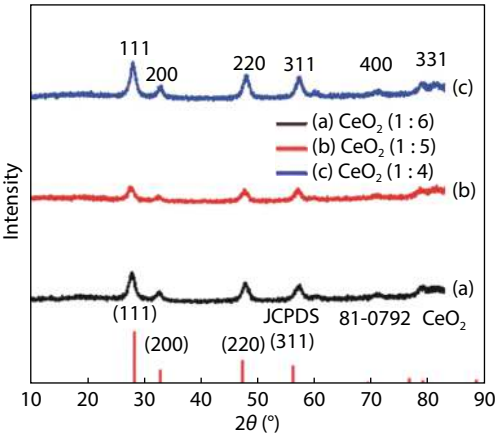

Fig. 1. (Color online) XRD patterns of the CeO_2 nano particles synthesized at different molar ratio.

Table 1. Crystal structure values of cerium oxide nanoparticles of different molar ratio.

Sample	Crystal size (nm)	Lattice parameter (Å)	
CeO_2 (1 : 6)	8.2	5.5262	Std-JCPDS 81-0792
CeO_2 (1 : 5)	6.2	5.5425	
CeO_2 (1 : 4)	6.0	5.5482	5.412

$$D = \alpha\lambda/\beta\cos\theta, \tag{4}$$

where D is the average grain size, α is a geometric factor (here, α = 0.9), λ is the wavelength of X-rays used for the measurements (λ = 1.54056 Å), β is the FWHM of the diffraction peaks, which can be measured from the XRD peaks and θ is the diffraction angle.

Table 1 displayed the crystalline structure and lattice parameters of CeO_2 NPs from XRD results. From Eq. (4) the calculated grain size are 8.2, 6.2 and 6.6 nm for different molar ratio (1 : 6), (1 : 5), (1 : 4) of NaOH respectively. The crystal size was reduced to 6.2 nm by lowering the sodium hydroxide concentration, but when the concentration is lowered higher, the crystal size gradually increases, it shows that 5 mmol concentration of NaOH is suitable to get the optimized crystal size of nano particles. The optimized concentration of NaOH acts as the oxidizing agent to get Ce (IV) oxide, which was confirmed by JCPDS file no: 81-0792 and elemental X-ray analysis.

3.2. SEM with EDXs analysis

The morphological studies of as synthesized CeO_2 NPs sample and the nano structures of the sample were examined by SEM shown in Fig. 2.

The mechanism of CeO_2 nano particles gives poly crystalline pore evaluation with crystal size ranges from 8.2 to 6.6 nm for different concentrations of NaOH solution. Figs. 2(a) and 2(c) show the uniform and large grain size with a sphere-like structure in the (1 : 6) and (1 : 4) concentration. It can be seen that there is some agglomeration due to strong attractive force among the particles, which develops thicker and longer nano particles that increases the size[41]. Another reason for the agglomeration is a fall on the presence of a high concentration of the hydroxyl group on the surface of its hydrothermal synthesis[42–44]. The proportion of cerium nitrate hexahydrate source material, continuously dehydrate and oxidize with the support of NaOH concentration, the ion regu-

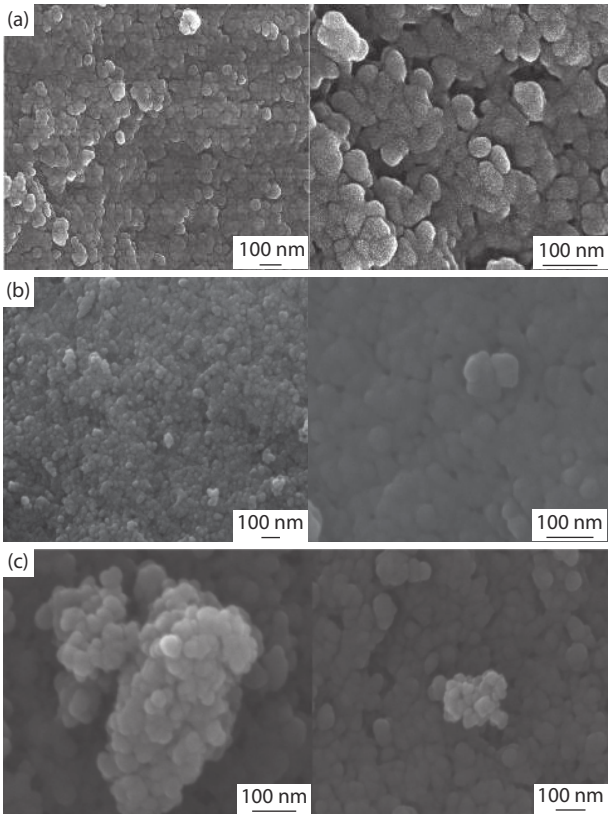

Fig. 2. SEM image of (a) CeO_2 (1 : 6), (b) (1 : 5), (c) (1 : 4).

lates the release of oxygen by Ce(IV) during the synthesis. As a result, Fig. 2(b) depicts the particle size distribution with CeO_2 NPs as the average size.

As seen in Fig. 3, the EDAX analysis showed the peaks of the elements and percentages of cerium and oxygen concentrations for the different concentrations of NaOH. There was no such a difference in the elemental analysis and its proportions, which helps in determining the stoichiometry elements in CeO_2 NPs. The information ensured that the cerium oxide formed by hydrothermal synthesis was CeO_2 nanoparticles.

3.3. UV–vis-diffuse reflectance spectra

Optical properties of the synthesized CeO_2 NPs studied by using UV–vis DRS. Fig. 4 shows the absorbance spectrum of synthesized CeO_2 NPs 200–800 nm wavelength range. The absorption edges of the CeO_2 nano cube were found near 440–443 nm range and a strong red shift is shown by the spectra.

The optical absorption near band gap energy E_g was calculated by using Tauc's formula is[45]:

$$(\alpha h\nu)^2 = A(h\nu - E_g), \tag{5}$$

where α is the absorption coefficient, $h\nu$ is the incident photon energy, A is the constant.

For direct transition, the plots of $(\alpha h\nu)^2$ versus $h\nu$ for CeO_2 NPs are shown in Figs. 5(a)–5(c). The direct band gap energy E_g was found from the intersection of extra polated linear portion. Figs. 5(a)–5(c) displayed the band gap energy values are 2.88, 2.82 and 2.87 eV for CeO_2 NPs with molar ratios (1 : 4), (1 : 5) and (1 : 6) respectively. The bandgap values suggested the semiconducting nature of synthesized CeO_2 NPs[46].

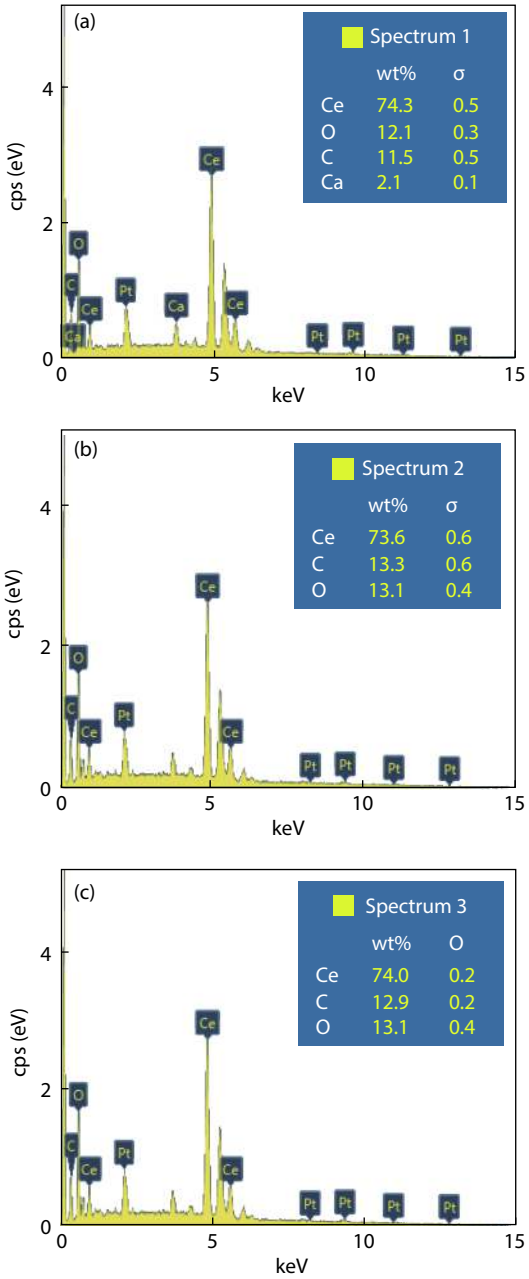

Fig. 3. (Color online) EDAX spectrum of (a) CeO_2 (1 : 6), (b) CeO_2 (1 : 5) and (c) CeO_2 (1 : 4).

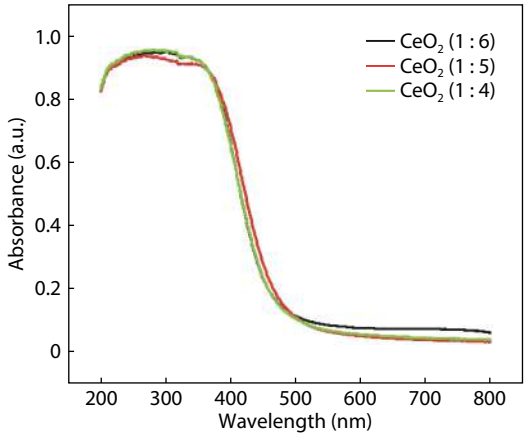

Fig. 4. (Color online) UV –vis absorbance spectra of as synthesised CeO_2.

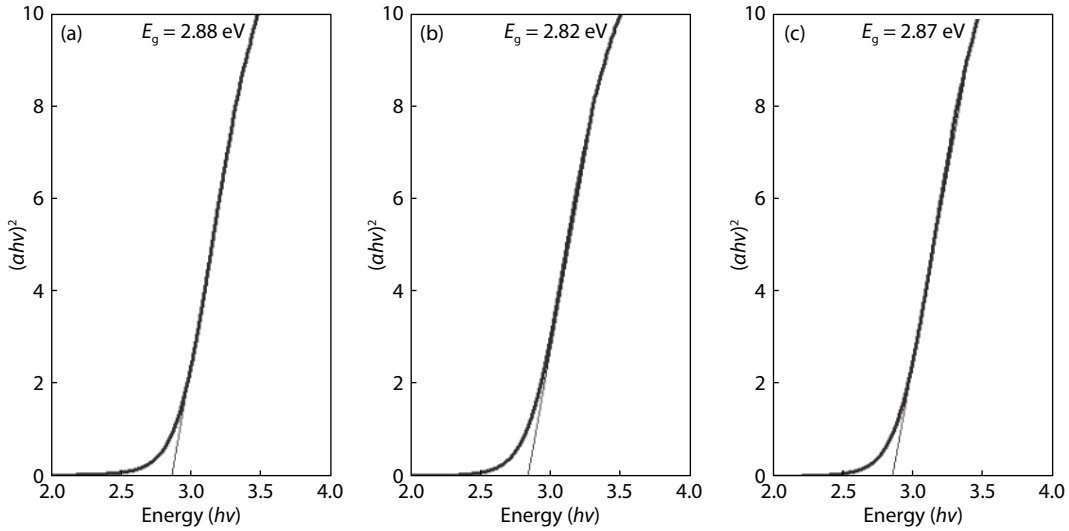

Fig. 5. UV–vis DRS of (a) ceria (1 : 6), (b) (1 : 5) and (c) (1 : 4) proportions of the samples.

Figs. 5(a)–5(c) depicted that the incorporated oxygen has improper light absorption of capacity of synthesized ceria nano particles. Stronger absorption lies in the region of 200 to 450 nm and the higher absorption of this region clearly states that ceria nano particle has a lower dye loading ability; its photocatalytic activity conforms with this improvement in light absorption of capacity in our second sample, which is excellent, and is mainly due to the incorporation of oxygen inside the sites[47].

3.4. XPS analysis

The composition and purity of the as-prepared ceria sample were studied by XPS analysis as shown in Fig. 6. Peaks of Ce 3d, O 1s, C 1s, and Ce 4d can be analysed using CASAXPS software. There were no peaks obtained for Na 2p, which indicate that there were no impurities of NaOH. XPS analysis also confirmed that as-synthesized nano particle contains Ce^{4+} ion and oxygen vacancies, which is shown in the normal mode of Fig. 6(a). However, the following figure specifically defined the binding energy peaks, which were consistent with previously published findings labeled in our Fig. 6(b) – the final state of Ce^{4+}[48]. From Fig. 6(b) the core level Ce 3d spectra of CeO_2 shows six contributions in which two types of Ce that is Ce(III) and Ce(IV) are presented. The peaks appeared at 925 and 891 eV, together with 922 and 897 eV, are weaker than 916 and 885 eV, and confirms the presence of Ce(IV). The high intensity and area of 925 eV can be attributed to the interaction between Ce and its surrounding atoms. Ce(III) can be considered as an indicator for the photo reduction reaction[44]. From Fig. 6(c), it is noted that the O 1s spectra of the products consist of three peaks at 529, 530.5, and 531.5 eV respectively. The peak at 529 eV can be attributed to lattice oxygen ion in CeO_2 like that the peak at 530.5 eV originated from absorbed oxygen another peak at 531.5 eV assigned to lattice oxygen ion if the synthesized cerium oxide nano particles is as CeO_2[49].

3.5. Raman spectroscopy

Fig. 7 exhibits that the Ce(IV) ion and oxygen vacancy contribute to the most intense peak around 466 cm^{-1} of the Raman peak position because there is no weaker peaks where detected for this CeO_2 nanoparticles. It can be attributed there

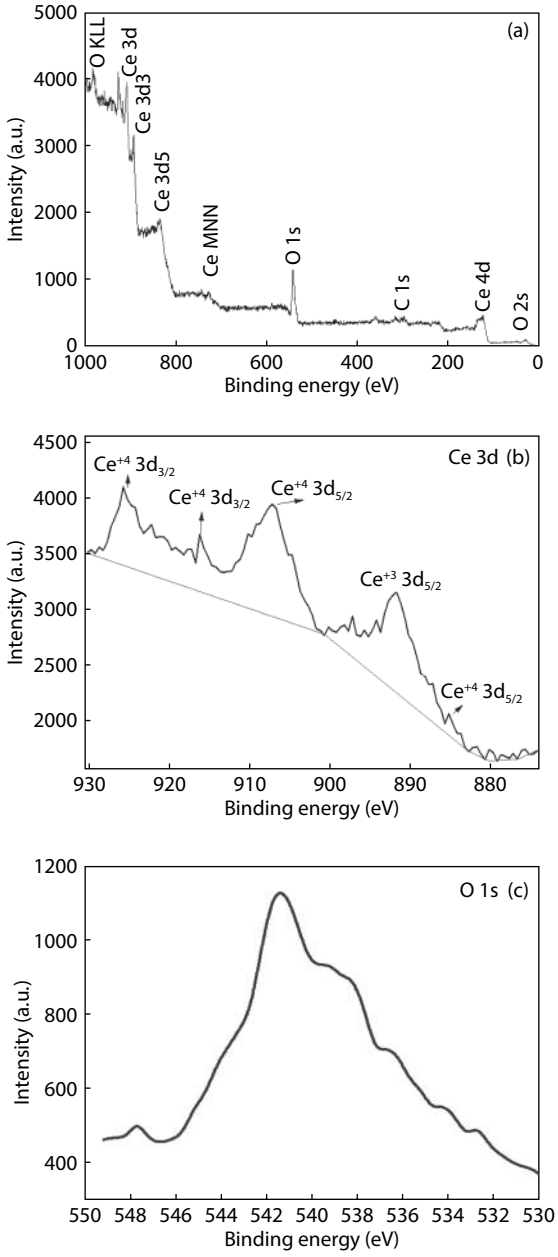

Fig. 6. X-Ray Photoelectron Spectra of ceria nanoparticles.

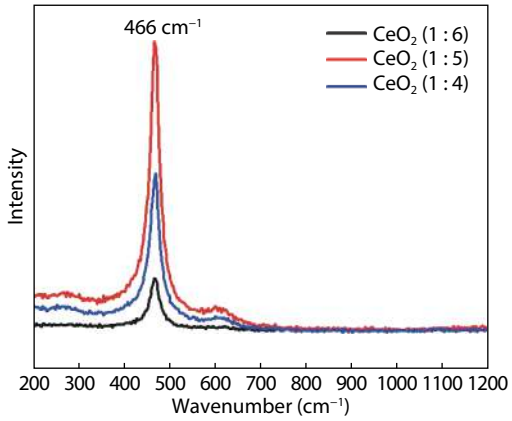

Fig. 7. (Color online) Raman spectra of synthesised ceria nanoparticles in different molar ratio.

is no ascribed broad band spectrum due to oxygen vacancy and defects caused by CeO_2 nanoparticles. The peak at 466 cm^{-1} is assigned to first-order Raman mode (F_{2g}) features of super oxides, which is already reported in the literature[50]. The reported results matched well with our intense peak.

Among the three samples, the concentration of oxygen vacancy is bigger than the higher concentration of Ce(IV) ion, which is well matched with spherical formula detected for the second sample. So, we can conclude that even the energy band is nearly 2.5 eV and red shift results of Ce(IV) ion and oxygen vacancy lead to a decrease in the binding of nanoparticles, which is the main reason of hydrothermal synthesis and its reaction time of 12 h. It is believed that there is no degree of oxygen defect for these three samples and it confirms that the increase in reaction time from 6 to 12 h enhances the above said properties of CeO_2 nanoparticles[51].

3.6. Photocatalytic degradation study

In order to investigate the photo catalytic degradation properties of as-prepared CeO_2 nano structured samples, MB was used as model pollutants to study the photo catalytic performance of CeO_2 NPs. The utmost absorptive energy of methylene blue was at 664 nm. Fig. 8 shows the schematic illustration of the possible photocatalytic reaction mechanism over CeO_2 NPs. The absorptive intensity of MB gradually decreases with the prolonging of the irradiation time when the mixed solution of MB and CeO_2 nanoparticles were exposed to UV-B light irradiation at room temperature. This result indicates that MB dye attains optimum degradation behaviour under the catalysis of CeO_2 nanoparticles.

More importantly, the CeO_2 (1 : 4, 1 : 5, 1 : 6 molar ratio of NaOH) nanoparticles dramatically enlarged the specific surface area calculated by BET analysis to 488, 492 and 490 m^2/g, together with an increase in micropore volume from 0.010, 0.310 and 0.206 cm^3/g, which is, in fact, much higher than the reported semiconductor-graphene composites or most of the porous photocatalysts[52].

The improved photocatalytic activity of CeO_2 (1 : 4, 1 : 5, 1 : 6 molar ratio of NaOH) nanoparticles under UV irradiation is attributed to high-surface-area, enhanced absorption of MB dyes, and more efficient separation of photogenerated electron–hole pairs. The transfer of photogenerated electrons from the surface of the samples reduces the possibility of decomposing Ce^{4+} for the recycling of CeO_2 photocatalyst[53, 54].

Figs. 9(a)–9(c). Photocatalytic degradation of absorbance spectrum of MB in the presence of CeO_2 (1 : 4, 1 : 5, 1 : 6 molar ratio), (catalyst dosage – 250 mg/250 mL, concentration of MB = 5 mg/L; light source = UV-B). The photo-catalyst produces surface oxidation to eliminate the colour effect of MB dye such as organic compounds when it is exposed to UV light. By applying the principle of degradation, dissolving O_2^- in the air, removing the colour is possible. Fig. 9(a) shows the shift in the absorbance wavelength is the energy that makes electrons jump up by UV light.

In order to transfer electrons from the valence band (VB) to the conduction band (CB) in CeO_2, the energy of light photons should be at least equal or higher than the energy of a band gap in the photocatalyst. CeO_2 has some energy (2.88 eV = 3.2 × 1.6 × 10^{-19} J) for (1 : 6) ratio, the necessary wavelength is nearly 430 nm, which tells us that the UV light needed this much of amount of energy to activate the photo catalyst for the degradation[55].

CeO_2 nanoparticles as photocatalysis effectively detoxify noxious organic pollutants. UV is used to create electron–hole pairs in the semiconducting oxide of CeO_2 NPs.

Electrons can react with oxygen adsorbed on the photocatalyst surface and then the formation of superoxide anion radicals is observed according to the following reaction:

$$CeO_2\left(e^-_{CB}\right) + O_2^- \rightarrow CeO_2 + O^{2\bullet-}$$

The radical species then attack the organic molecule, which is eventually oxidized to CO_2, H_2O, and HCl if the organic molecule contains chlorine[56].

One of the most critical controlling elements in the generation of reactive oxide species is the location of edges in CB and VB (ROS). Because the locations of CB and VB in CeO_2 include the possibility for the generation of hydroxyl radicals and superoxide anion radicals (Fig. 8). The major reactive oxygen species (ROS) produced in the photocatalytic system in water oxidation by photogenerated holes (h^+) and oxygen reduction by photoexcited electrons (e) in CB are hydroxyl radicals ($OH^\bullet$) and superoxide anion radicals ($O^{2\bullet}$). These species, like hydroperoxide radicals ($HO^{2\bullet}$), are extremely reactive and can contribute to the photocatalytic degradation of contaminants in industrial effluent[57, 58]. The absorbance of photocatalytic efficiency of CeO_2 NPs have more surface energy because of its smaller particle size, which could be already observed 8.2 nm. The band gap energy of CeO_2 nearly equal to 2.88 eV and its band edges shifted for the different NaOH concentrations of its preparation to yield larger redox potential. This indicates that the electronegative $CeO_{2\ surface}$ creates a stronger dipole moment with the oxygen molecules; the dye added for the degradation technique is MB. A hybridization effect can retard the recombination of the electron–hole pair and increases the inhibition properties of the photo catalytic nano particles of the prepared solution. Here, we concluded that the prepared CeO_2 nanoparticles have a synergetic effect of quantum confinement and a large surface-to-volume ratio which contributes to the enhanced photo degradation of MB. Fig. 10 shows the absorption characteristics of MB (C_0 = 5 mg/L) onto the surface of CeO_2 nanoparticles for the concentration of MB after dark adsorption and UV–vis absorption were investigated. After equilibrium in the dark adsorption, for every 30 min only 5% of MB was adsorbed on the CeO_2 NPs surface, which were already reported[59].

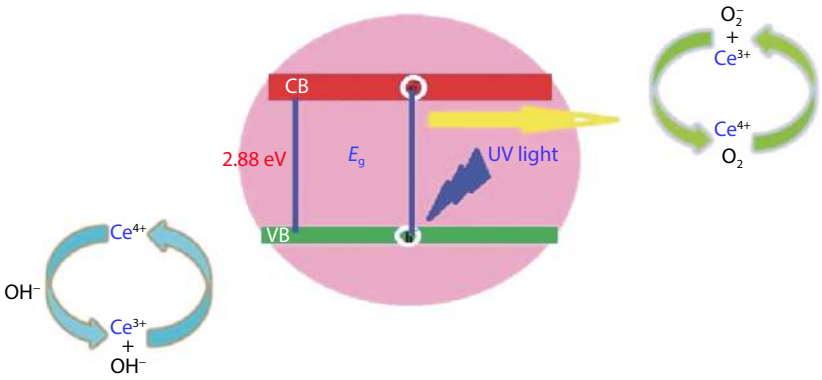

Fig. 8. (Color online) Mechanism of Photocatalytic degradation of MB dye.

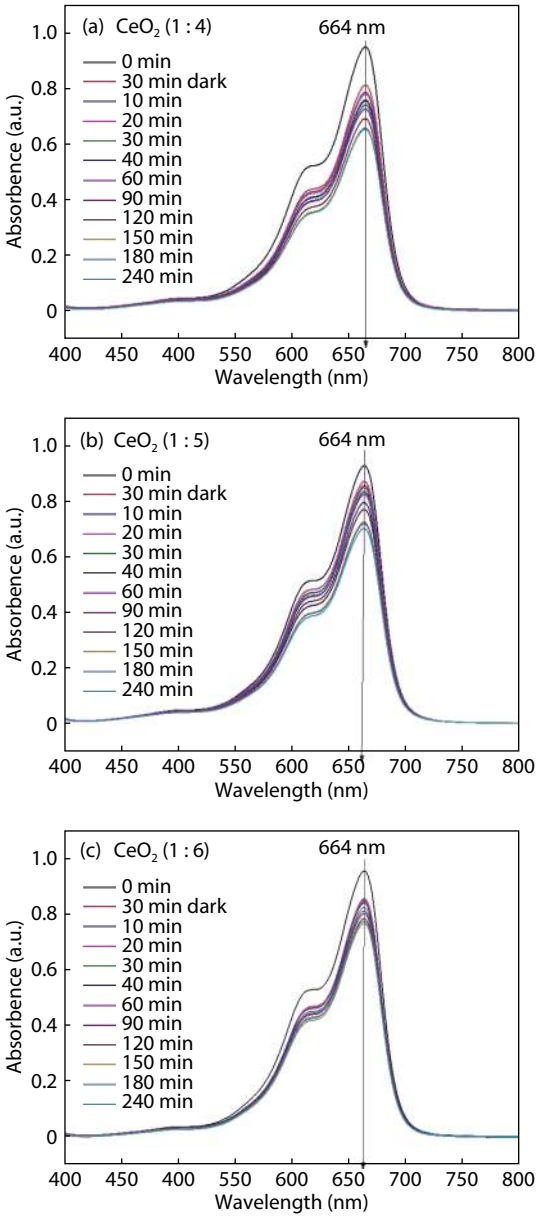

Fig. 9. (Color online) Photocatalytic degradation of absorbance spectrum of MB in the presence of CeO_2 (1 : 4, 1 : 5, 1 : 6 molar ratio). (catalyst dosage – 250 mg/250 mL, concentration of MB = 5 mg/L; light source = UV-B)

Under light irradiation, the dyes are excited and then photo-generated electrons could easily transfer into the CeO_2 surface and effectively participated in the redox reaction of CeO_2 nanoparticles. Fig. 10 shows the variation of normalized concentration of MB (C_0 = 5 mg/L) with irradiation time under UV–light condition. This figure revealed the effect of absorptivity and photo reactivity resulting in an appreciable improvement in the photo degradation of MB with CeO_2 nanoparticles. Here CeO_2 nanoparticles served as an electron acceptor and conductor due to its one-dimensional structure, which helps or suppress charge recombination, enhancing charge separation efficiency and improving photo catalytic activities. The excellent electron factors can enhance the photo catalytic activity of nano-sized CeO_2, high dye adsorptivity and high electron conduction to remove the dye molecules by the process of photo degradation.

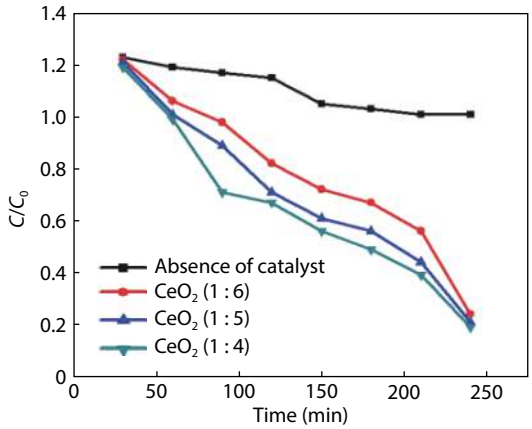

Fig. 10. (Color online) Variation of normalized concentration of MB (C_0 = 5 mg/L) with irradiation time under UV–light condition.

When the particle size of CeO_2 is decreased to a nanoscale and applied in the form of nanostructures, the characteristics of the material can be drastically altered. CeO_2 features such as lattice symmetry, cell parameters, and structural features are all affected by this process. In their bulk form, phases have a high surface energy and are unstable. The surface energy of nanostructured CeO_2 materials dramatically reduces as the particle size is decreased to the nanoscale, and nanostructured materials have a high level of stability[60]. In addition, hydrothermally prepared ceria nanoparticles have a high catalytic activity, which is due to the rapid mobility of surface oxygen vacancies.

4. Conclusion

CeO_2 NPs were successfully synthesized using an effi-

cient hydrothermal process with three different NaOH precipitating agent molar ratios. Depending on the reaction time and NaOH concentration, CeO_2 NPs had different crystal sizes and lattice parameters. Under MB, the prepared CeO_2 NPs' photodegradation activity was characterized and evaluated. The crystal size was reported to be 8.2, 6.2, and 6.6 nm, with a cubic structure. The band gap values of 2.87, 2.82, and 2.88 eV were measured using a UV–vis spectrometer to describe the optical properties. Its value is lower than the bulk value of CeO_2. In the (1 : 6) and (1 : 4) molar ratios, these CeO_2 NPs are all spherical, with heavy agglomeration. The grain size of the (1 : 5) sample is unique in nature, and its best morphological structure justified that this composition is stronger in terms of Ce(IV) and oxygen ion composition, and XRD tests concluded that it is a single crystalline cubic cerium (IV) oxide nano particle. Oxygen defects decrease as reaction time (6–12 h) increases in two samples (1 : 6) and (1 : 4), respectively. Under UV light irradiation, the photocatalytic degradation behavior of MB dye shows that hydrothermally prepared CeO_2 NPs are an efficient photo catalyst.

References

[1] Mogensen M, Sammes N M, Tompsett G A. Physical, chemical and electrochemical properties of pure and doped ceria. Solid State Ion, 2000, 129, 63

[2] Yashima M, Sasaki S, Yamaguchi Y, et al. Internal distortion in ZrO_2-CeO_2 solid solutions: Neutron and high-resolution synchrotron X-ray diffraction study. Appl Phys Lett, 1998, 72, 182

[3] Feng X, Sayle D C, Wang Z L, et al. Converting ceria polyhedral nanoparticles into single-crystal nanospheres. Science, 2006, 312, 1504

[4] Yamashita K. Hydrothermal synthesis and low temperature conduction properties of substituted ceria ceramics. Solid State Ion, 1995, 81, 53

[5] Imanaka N, Masui T, Hirai H, et al. Amorphous cerium–titanium solid solution phosphate as a novel family of band gap tunable sunscreen materials. Chem Mater, 2003, 15, 2289

[6] Kubacka A, Fernández-García M, Colón G. Advanced nanoarchitectures for solar photocatalytic applications. Chem Rev, 2012, 112, 1555

[7] Yu J, Wang S, Low J, et al. Enhanced photocatalytic performance of direct Z-scheme g-C_3N_4-TiO_2 photocatalysts for the decomposition of formaldehyde in air. Phys Chem Chem Phys, 2013, 15, 16883

[8] Miranda C, Mansilla H, Yáñez J, et al. Improved photocatalytic activity of g-C_3N_4/TiO_2 composites prepared by a simple impregnation method. J Photochem Photobiol A, 2013, 253, 16

[9] Muñoz-Batista M J, Kubacka A, Fernández-García M. Effect of g-C_3N_4 loading on TiO_2-based photocatalysts: UV and visible degradation of toluene. Catal Sci Technol, 2014, 4, 2006

[10] Murrell L L, Tauster S J, Anderson D R. Laser Raman characterization of surface phase precious metal oxides formed on CeO_2. Stud Surf Sci Catal, 1991, 71, 275

[11] Hussain K, Hussain T. Gold nanoparticles: A boon to drug delivery system. South Ind J Biol Sci, 2015, 1, 128

[12] Ali F S, Qi K Z, Al Wahaibi B, et al. Photocatalytic degradation of bisphenol A in the presence of TiO_2 nanoparticle: Effect of solvent on size control. Desal Water Treat, 2017, 79, 301

[13] Qi K Z, Selvaraj R, Al Fahdi T, et al. Enhanced photocatalytic activity of anatase-TiO_2 nanoparticles by fullerene modification: A theoretical and experimental study. Appl Surf Sci, 2016, 387, 750

[14] Zhang Y F, Selvaraj R, Sillanpää M, et al. Enhanced solar photocatalytic activity of Er^{3+}:$YAlO_3$-loaded $BiPO_4$ composite. J Ind Eng Chem, 2015, 24, 161

[15] Sim J H, Umh H N, Shin H H, et al. Comparison of adsorptive features between silver ion and silver nanoparticles on nanoporous materials. J Ind Eng Chem, 2014, 20, 2864

[16] Mokkelbost T, Kaus I, Grande T, et al. Combustion synthesis and characterization of nanocrystalline CeO_2-based powders. Chem Mater, 2004, 16, 5489

[17] Maric R, Oljaca M, Vukasinovic B, et al. Synthesis of oxide nanopowders in nano spray diffusion flames. Mater Manuf Process, 2004, 19, 1143

[18] Kockrick E, Schrage C, Grigas A, et al. Synthesis and catalytic properties of microemulsion-derived cerium oxide nanoparticles. J Solid State Chem, 2008, 181, 1614

[19] Mädler L, Stark W J, Pratsinis S E. Flame-made ceria nanoparticles. J Mater Res, 2002, 17, 1356

[20] Laberty-Robert C, Long J W, Lucas E M, et al. Sol–gel-derived ceria nanoarchitectures: Synthesis, characterization, and electrical properties. Chem Mater, 2006, 18, 50

[21] Cho M Y, Roh K C, Park S M, et al. Control of particle size and shape of precursors for ceria using ammonium carbonate as a precipitant. Mater Lett, 2010, 64, 323

[22] Gulicovski J J, Milonjić S K, Szécsényi K M. Synthesis and characterization of stable aqueous ceria sols. Mater Manuf Process, 2009, 24, 1080

[23] Hirano M, Inagaki M. Preparation of mono disperse cerium (IV) oxide particles by thermal hydrolysis. J Mater Chem, 2000, 10, 473

[24] Cui R R, Lu W C, Zhang L M, et al. Template-free synthesis and self-assembly of CeO_2 nanospheres fabricated with foursquare nanoflakes. J Phys Chem C, 2009, 113, 21520

[25] Athawale A A, Bapat M S, Desai P A. Hydroxide directed routes to synthesize nanosized cubic ceria (CeO_2). J Alloys Compd, 2009, 484, 211

[26] Sahoo S K, Mohapatra M, Singh A K, et al. Hydrothermal synthesis of single crystalline nano CeO_2 and its structural, optical, and electronic characterization. Mater Manuf Process, 2010, 25, 982

[27] Zhai Y Q, Zhang S Y, Pang H. Preparation, characterization and photocatalytic activity of CeO_2 nanocrystalline using ammonium bicarbonate as precipitant. Mater Lett, 2007, 61, 1863

[28] Zhou Y C, Rahaman M N. Hydrothermal synthesis and sintering of ultrafine CeO_2 powders. J Mater Res, 1993, 8, 1680

[29] Nikolaou K. Emissions reduction of high and low polluting new technology vehicles equipped with a CeO_2 catalytic system. Sci Total Environ, 1999, 235, 71

[30] Goharshadi E K, Samiee S, Nancarrow P. Fabrication of cerium oxide nanoparticles: Characterization and optical properties. J Colloid Interface Sci, 2011, 356, 473

[31] Khan M M, Ansari S A, Pradhan D, et al. Defect-induced band gap narrowed CeO_2 nanostructures for visible light activities. Ind Eng Chem Res, 2014, 53, 9754

[32] Zheng X G, Huang S, Yang D M, et al. Synthesis of X-architecture CeO_2 for the photodegradation of methylene blue under UV-light irradiation. J Alloys Compd, 2017, 705, 131

[33] Li S J, Wang C C, Liu Y P, et al. Photocatalytic degradation of antibiotics using a novel Ag/Ag_2S/Bi_2MoO_6 plasmonic p-n heterojunction photocatalyst: Mineralization activity, degradation pathways and boosted charge separation mechanism. Chem Eng J, 2021, 415, 128991

[34] Li S J, Chen J L, Hu S W, et al. Facile construction of novel Bi_2WO_6/Ta_3N_5 Z-scheme heterojunction nanofibers for efficient degradation of harmful pharmaceutical pollutants. Chem Eng J, 2020, 402, 126165

[35] Li S J, Xue B, Chen J L, et al. Constructing a plasmonic p-n heterojunction photocatalyst of 3D Ag/$Ag_6Si_2O_7$/Bi_2MoO_6 for efficiently

removing broad-spectrum antibiotics. Sep Purif Technol, 2021, 254, 117579
[36] Li S J, Hu S W, Jiang W, et al. *In situ* construction of WO_3 nanoparticles decorated Bi_2MoO_6 microspheres for boosting photocatalytic degradation of refractory pollutants. J Colloid Interface Sci, 2019, 556, 335
[37] Dong B, Li L Y, Dong Z F, et al. Fabrication of CeO_2 nanorods for enhanced solar photocatalysts. Int J Hydrog Energy, 2018, 43, 5275
[38] Wang L N, Meng F M, Li K K, et al. Characterization and optical properties of pole-like nano-CeO_2 synthesized by a facile hydrothermal method. Appl Surf Sci, 2013, 286, 269
[39] Klug H P, Alexandef L E. X-ray diffraction procedures. New York: Wiley, 1974, 689.
[40] Lin M, Fu Z Y, Tan H R, et al. Hydrothermal synthesis of CeO_2 nanocrystals: Ostwald ripening or oriented attachment. Cryst Growth Des, 2012, 12, 3296
[41] Jawor-Baczynska A, Moore B D, Sefcik J. Effect of mixing, concentration and temperature on the formation of mesostructured solutions and their role in the nucleation of dl-valine crystals. Faraday Discuss, 2015, 179, 141
[42] Vekilov P G. The two-step mechanism of nucleation of crystals in solution. Nanoscale, 2010, 2, 2346
[43] Tauc J C. Amorphous and liquid semiconductors. London: Plenum Press 1974
[44] Wang Z L, Quan Z W, Lin J. Remarkable changes in the optical properties of CeO_2 nanocrystals induced by lanthanide ions doping. Inorg Chem, 2007, 46, 5237
[45] Wang X Y, Tian J J, Fei C B, et al. Rapid construction of TiO_2 aggregates using microwave assisted synthesis and its application for dye-sensitized solar cells. RSC Adv, 2015, 5, 8622
[46] Lu F, Meng F M, Wang L N, et al. Morphology-selective synthesis method of nanopolyhedra and square-like CeO_2 nanoparticles. Mater Lett, 2012, 73, 154
[47] Li C R, Zhang X Q, Dong W J, et al. High photocatalytic activity material based on high-porosity ZnO/CeO_2 nanofibers. Mater Lett, 2012, 80, 145
[48] Li S N, Zhu H Q, Qin Z F, et al. Catalytic performance of gold supported on mn, Fe and Ni doped ceria in the preferential oxidation of CO in H_2-rich stream. Catalysts, 2018, 8, 469
[49] Palmqvist A E C, Wirde M, Gelius U, et al. Surfaces of doped nanophase cerium oxide catalysts. Nanostruct Mater, 1999, 11, 995
[50] Weber W H, Hass K C, McBride J R. Raman study of CeO_2: Second-order scattering, lattice dynamics, and particle-size effects. Phys Rev B, 1993, 48, 178
[51] Lu X H, Huang X, Xie S L, et al. Facile electrochemical synthesis of single crystalline CeO_2 octahedrons and their optical properties. Langmuir, 2010, 26, 7569
[52] Wang S L, Xu M, Peng T Y, et al. Porous hypercrosslinked polymer-TiO_2-graphene composite photocatalysts for visible-light-driven CO_2 conversion. Nat Commun, 2019, 10, 676
[53] Yang X F, Cui H Y, Li Y, et al. Fabrication of Ag_3PO_4-graphene composites with highly efficient and stable visible light photocatalytic performance. ACS Catal, 2013, 3, 363
[54] Chai R J, Li Y K, Zhang Q F, et al. Monolithic Ni-MO_x/Ni-foam (M = Al, Zr or Y) catalysts with enhanced heat/mass transfer for energy-efficient catalytic oxy-methane reforming. Catal Commun, 2015, 70, 1
[55] Solsona B, Concepción P, Hernández S, et al. Oxidative dehydrogenation of ethane over NiO-CeO_2 mixed oxides catalysts. Catal Today, 2012, 180, 51
[56] Zhang Z Q, Han L P, Chai R J, et al. Microstructured CeO_2-NiO-Al_2O_3/Ni-foam catalyst for oxidative dehydrogenation of ethane to ethylene. Catal Commun, 2017, 88, 90
[57] Kohantorabi M, Gholami M R. Kinetic analysis of the reduction of 4-nitrophenol catalyzed by CeO_2 nanorods-supported CuNi nanoparticles. Ind Eng Chem Res, 2017, 56, 1159
[58] Liang Y, Chen Z, Yao W, et al. Decorating of Ag and CuO on Cu nanoparticles for enhanced high catalytic activity to the degradation of organic pollutants. Langmuir, 2017, 33, 7606
[59] Park S, Park J, Selvaraj R, et al. Facile microwave-assisted synthesis of SnS_2 nanoparticles for visible-light responsive photocatalyst. J Ind Eng Chem, 2015, 31, 269
[60] Capodaglio A. Contaminants of emerging concern removal by high-energy oxidation-reduction processes: State of the art. Appl Sci, 2019, 9, 4562

Fowziya Shaik Ali has completed her PhD (in Nanochemistry) during 2019 and she is working as Assistant Professor of Chemistry at Khadir Mohideen College, Adirampattinam. She has published more than five articles in Scopus indexed journals and has only one patent copyright in her credit.

A. Ayeshamariam is working in the Research Department of Physics, Khadir Mohideen College, Adirampattinam. She received her MSc (Physics) and PhD (Nanoscience) from Alagappa University, Karaikudi. She has completed two minor research projects sponsored by UGC, Hyderabad, and one short-term research project sponsored by INUP, IIT, Bombay. Her main research interests are materials science, the study of nano-oxide semiconductors, thin film preparation techniques, materials characterization, environmental water and air pollution control, thin film coatings for bio-medical application and solar energy devices/systems. She has published four book chapters. She is co-author of 76 papers.